Available online at www.sciencedirect.com

ScienceDirect

Ceramics International 42 (2016) 5011–5017

CERAMICS INTERNATIONAL

www.elsevier.com/locate/ceramint

Structural, magnetic and Mössbauer study of $BaLa_xFe_{12-x}O_{19}$ nanohexaferrites synthesized via sol–gel auto-combustion technique

Virender Pratap Singh[a,b,*], Gagan Kumar[c], Arun Kumar[a], Radhey Shyam Rai[b], M.A. Valente[d], Khalid M. Batoo[e], R.K. Kotnala[f], M. Singh[a]

[a]Department of Physics, Himachal Pradesh University, Shimla, India
[b]School of Physics, Shoolini University, Bajhol, Solan, India
[c]Department of Physics, IEC University, Atal Nagar, Kallujhanda, Baddi, India
[d]Department of Physics, University of Aveiro, 3810-193 Aveiro, Portugal
[e]King Abdullah Institute for Nanotechnology, King Saud University, Riyadh, Saudi Arabia
[f]CSIR—National Physical Laboratory, Dr. K.S. Krishnan Marg, New Delhi 110012, India

Received 11 October 2015; received in revised form 25 November 2015; accepted 1 December 2015
Available online 24 December 2015

Abstract

$BaLa_xFe_{12-x}O_{19}$ ($0.05 \leq x \leq 0.25$) nanohexaferrites were synthesized by sol–gel auto combustion method. X-ray diffraction study revealed the hexagonal structure of the synthesized nanoferrites without any secondary phase and Rietveld analysis confirmed the P63/mmc space group. The crystallite size was observed to increase (49–63 nm) with the increasing substitution of La^{3+} ions. The particle size was observed to be in the range 49–63 nm. The remarkable increase in saturation magnetization upto 78.5 emu/g and an increase in magneto-crystalline anisotropic was observed with the increase in La^{3+} substitution. In addition, for the first time we have reported the Mösssbauer study of $BaLa_xF_{12-x}O_{19}$ nanohexaferrites in the present paper.

Keywords: Nanoparticles; Magnetic materials; Mössbauer analysis; Sol–gel preparation

1. Introduction

The landmark lecture in the history of nanoscience was first of all delivered by Feynman entitled as "There is a plenty of rooms at the bottom". Nanotechnology is directed toward understanding and creating improved materials, devices, and systems that exploit these new properties. Keeping in view these targets, material science research is focused on the invention of new materials with enhanced properties and novel synthesis techniques [1]. Nanocrystalline materials are in focus to recent scientific research because of their prospective applications and fascinating physics involved in them [2]. Bulk materials have constant physical properties regardless of its size, but at the nano-scale, size-dependent properties are often observed. Thus, the properties of materials change as their size approaches the nanoscale and as the percentage of atoms at the surface of a material becomes significant. Ferrites are the ceramic compounds with much high electrical resistivity than the metallic ferromagnetic materials. Ferrites reduce the eddy current losses and also absorb the electromagnetic field penetration.

Ferrites can be divided into three categories namely spinel, hexagonal and garnets according to their crystal lattice structure. Hexaferrites belong to the categories of hard ferrites, and are of different types depending upon the crystal structure and their chemical formula [3]. Out of various categories of hard ferrites; especially M-type hexaferrites are very intensively studied, because of their excellent behavior of magnetism. The keen interest of many material scientists on these hard ferrites is due to their potential applications at ultra-high frequency regions, like microwave antennas, wireless communications, radar technologies, and high magnetic storage devices [4]. The $BaFe_{12}O_{19}$ is M-type

*Corresponding author at: Department of Physics, Himachal Pradesh University, Shimla, India. Tel.: +91 9816714076.
E-mail address: kunwar.virender@gmail.com (V.P. Singh).

http://dx.doi.org/10.1016/j.ceramint.2015.12.014
0272-8842/

hexaferrite and belong to magnetoplumbite group. The unit cell of hexaferrites contains 19 O^{2-} ions & 1 Ba^{2+} ion and 12 Fe^{3+} ions. The Fe^{3+} ions are distributed among octahedral (12k, 2a, $4f_2$), tetrahedral ($4f_1$) and trigonal bipyramidal site (2b).

In hexaferrites, the electrical and magnetic properties mainly depend on the synthesizing technique, type of metal ions and their distribution between the different interstitial sites. Now-a-days due to the changing nature of day to day technologies, there is a need of materials which must have a high saturation magnetization, high coercivity, high magnetic anisotropy, excellent chemical stability, high natural resonant frequency and good capability of absorbing the unwanted electromagnetic signals. All these properties stated above are possessed by $BaFe_{12}O_{19}$ nanohexaferrite so M-type ferrites has been investigated during the last few years intensively and become one of the most high-tech materials. Due to larger intrinsic magneto-crystalline anisotropy M-type Barium nanoheaxferrite can be used at much higher frequency than the ferrites with spinel and garnet structure [5].

Many research workers have investigated substituted M-Type hard ferrites in the bulk form viz. Alam et al. [6] reported the decrease in magnetization (84.53 – 52.81 emu/g), and coercivity (3750 – 440 Oe) for the simultaneous substitution of Co^{2+}, Zn^{2+}, and Zr^{4+} ions in $BaFe_{12}O_{19}$ nanohexaferite processed via co-precipitation method, Chawla et al. [7] reported the decrease in magnetization (62.45 – 56.94 emu/g), and coercivity (5428.32 – 630.21 Oe) for the simultaneous substitution of Co^{2+}, and Zr^{4+} ions in $BaFe_{12}O_{19}$ nanohexaferite synthesized via sol–gel technique, Lee et al. [8] reported very low values of coercivity for $BaFe_{9.6}Co_{1.2}Ti_{1.2}O_{19}$ hexaferite synthesized via ball-milling and two step sintering processes. Li et al. [9] reported M_s=77.188 emu/g and H_c=4324 Oe for $BaFe_{12}O_{19}$ nanohexaferrite, and for pure as well as La^{3+} substitution they have not obtained quality hysteresis curves. Dhage et al. [10] reported the decrease in magnetization (40.443 – 5.12 emu/g), and coercivity (5689.28 – 5396.41 Oe) for the Cr^{3+} substituted $BaFe_{12}O_{19}$ nanohexaferites synthesized via sol–gel auto combustion method. Although, the structural and magnetic properties of substituted $BaFe_{12}O_{19}$ hexaferrites studied extensively [6–10], the available literature on lanthanum doped M-type nanohexaferrites is very scarce [7,9–10]. Keeping in mind the technological importance of M-type hexaferrites we have investigated the effects of La^{3+} ions on the structural, magnetic, and Mössbauer properties of sol–gel synthesized $BaFe_{12}O_{19}$ nanohexaferrites.

2. Experimental

2.1. Materials synthesis

Nanohexaferrites with a chemical formula $BaLa_xFe_{12-x}O_{19}$, where x=0.05, 0.1, 0.15, 0.2 and 0.25, were synthesized by the sol–gel auto-combustion technique. In a stoichiometric ratio, $Ba(NO_3)_3 \cdot 9H_2O$ $La(NO_3)_3 \cdot 6H_2O$ and $Fe(NO_3)_3 \cdot 9H_2O$ were dissolved in 30 ml of citric solution. The different pH values were taken into account but finally the pH value 7 was chosen in the present work as it gave the optimum results. The system was then heated at 80 °C with constant stirring until the wet gel was formed. The formed wet gel was then inflated resulting into black powder. The obtained powder was then sintered at 1100 °C for 4 h.

2.2. Instrumental details

The single-phase nature of the prepared samples is checked by X-ray diffraction (XRD) studies, which are made by Cu-K_α radiation of wavelength 1.54 Å using XPERT-PRO X-ray diffractometer. The transmission electron micrographs of all the samples were taken by using QUANTA 250 FFID 9393. The measurement of magnetization as a function of applied field was carried out by using the Lake Shore's Vibrating Sample Magnetometer. The room-temperature Mössbauer analysis was carried out by FAST Com Tec 070906 and the spectra were analyzed by MossWinn 4.0 software.

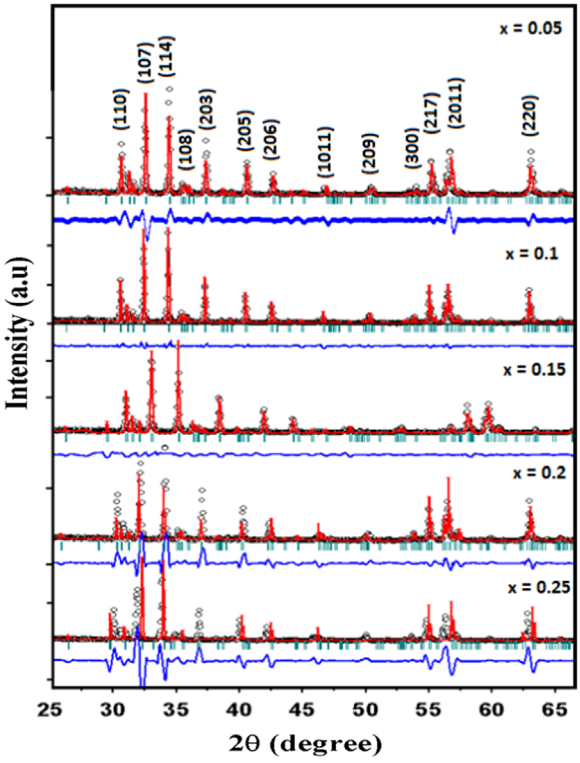

Fig. 1. Rietveld refined X-ray diffraction patterns of $BaLa_xFe_{12-x}O_{19}$ nanohexaferrites.

Table 1
Crystallite size, lattice parameter (a, c), c/a ratio, cell volume and X-ray density for $BaLa_xFe_{12-x}O_{19}$ nanohexaferrites.

x	t (nm)	a (Å)	c (Å)	c/a	V (Å^3)	d (g/cm^3)
0.05	49	5.890	23.19	3.94	696.71	5.337
0.1	55	5.894	23.21	3.94	698.25	5.365
0.15	56	5.894	23.21	3.94	698.25	5.404
0.2	62	5.895	23.22	3.94	698.79	5.440
0.25	63	5.907	23.32	3.95	704.66	5.434

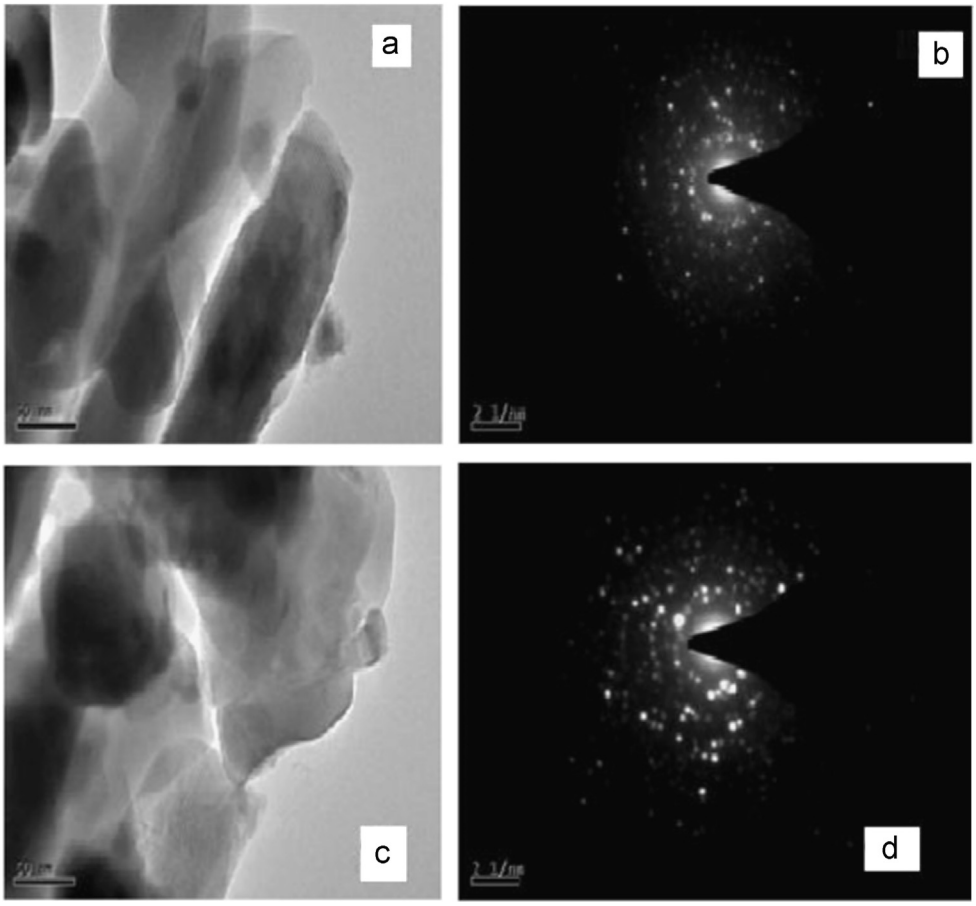

Fig. 2. (a) TEM and (b) SAED images for $BaLa_{0.15}Fe_{11.85}O_{19}$ nanohexaferrite, (c) TEM and (d) SAED images for $BaLa_{0.35}Fe_{11.75}O_{19}$ nanohexaferrite.

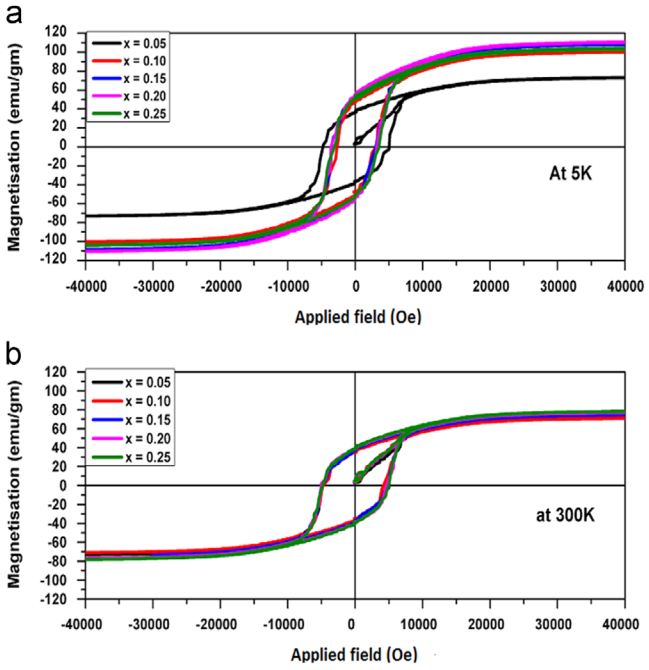

Fig. 3. M-H curves for $BaLa_xFe_{12-x}O_{19}$ nanohexaferrites at (a) 5 K and (b) 300 K.

Table 2
Compositional variation of saturation magnetization, coercivity, retentivity and squareness ratio for $BaLa_xFe_{12-x}O_{19}$ nanohexaferrites.

x	M_s (emu/g)	H_c (Oe)	M_r (emu/g)	Squareness ratio
0.05	72	5025	37	0.51
0.1	73	4194	35	0.48
0.15	74	5019	37	0.50
0.2	77	4628	38	0.49
0.25	78	4981	39	0.50

3. Results and discussion

3.1. Structural study

Fig. 1 shows the Rietveld refined X-ray diffraction patterns for all the nanohexaferrites. The peak position and relative intensity of all diffraction peaks are observed to be matching well with the standard powder diffraction file of JCPDS Card no. 84-0757 thereby confirming the magnetoplumbite phase of the P63/mmc space group. It is worth to mention here that other researchers [9,11–12] have shown the existence of secondary phase with the

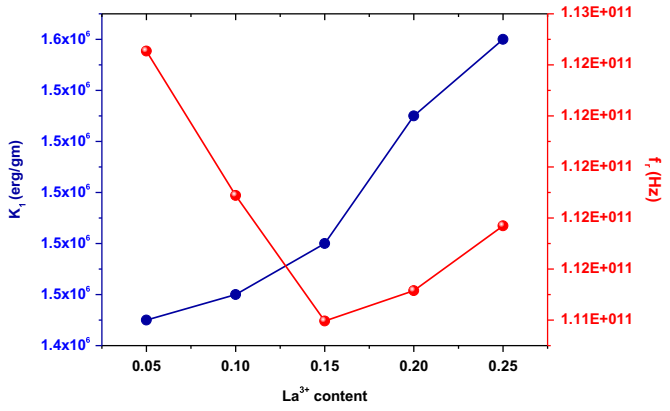

Fig. 4. Variation of magneto-crystalline anisotropy and resonant frequency as a function of La^{3+} ion content.

substitution of La^{3+} ions. Therefore, in the present work no such phase was observed thereby indicating the homogeneity of the synthesized nanohexaferrites.

The average crystallite size was calculated from the peak positions (114) and (107) using the Scherrer formula [13]

$$t = \frac{0.9\lambda}{\beta \cos \theta} \tag{1}$$

where t is the crystallite size in nm, β is full width at half maximum (FWHM), θ is the peak position in radian and λ is the wavelength. The lattice parameters 'a' and 'c' and density was calculated by using the following relations [14]:

$$\frac{1}{d^2} = \frac{4}{3}\frac{h^2+hk+k^2}{a^2} + \frac{l^2}{c^2} \tag{2}$$

$$d_x = \frac{2M}{N_a V_{cell}} \tag{3}$$

The calculated values of crystallite size, lattice parameters and density are given in Table 1. An increase in the particle size (49–63 nm), lattice parameter 'a' (5.890–5.907 Å) and 'c' (23.19–23.32 Å) was observed with the incorporation of La^{3+} ions. The lattice parameters were observed to increase because of the difference in ionic radius of La^{3+} (1.15 Å) as compared to that of Fe^{3+} (0.67 Å) ions. As La^{3+} ions replaced the Fe^{3+} ions thereby resulted in an internal stress to make the lattice distorted and an expansion of the unit cell. The density was also observed to increase with the incorporation of La^{3+} ions and can be correlated to the volume as well as increase in molecular weight. In order to confirm the particle size TEM measurement was carried out and is shown in Fig. 2. It is evident that the average size is in between 45 and 60 nm.

3.2. Magnetic study

In order to investigate the magnetic response of the prepared samples to an external field, we measured field dependent magnetization of samples at 5 K and 300 K and results are shown in Fig. 3(a) and (b) respectively and the values are given in Table 2. At room temperature, saturation magnetization was observed to increase (72–78 emu/g) with the incorporation of La^{3+} ions and the same has suggested the strengthening of the exchange interactions with the increasing substitution of La^{3+} ions. In M-type nanohexaferrites, the Fe^{3+} ions are distributed over three interstitial sites, tetrahedral, octahedral and trigonal bipyramidal, which are further divided into different sub-lattices [14]. Tetrahedral site has only $4f_1$ sub-lattice which has two Fe^{3+} ions in spin down state. Octahedral site is divided into three sub-lattices (12k, 2a and $4f_2$). Out of three sub-lattices, 12k has six Fe^{3+} ions and $4f_2$ sub-lattice has two Fe^{3+} ions in spin up state while 2a sub-lattice has one Fe^{3+} ion in spin down state. Trigonal bipyramidal site has only 2b sub-lattice which has one Fe^{3+} ion in spin down state. The net magnetic moment in M-type hexaferrites is given by the following relation [14]:

$$M_{Total}(T) = [6M_{12k}(T) + 1M_{2b}(T) + 1M_{2a}(T)]\uparrow - [2M_{4f1}(T) + 2M_{4f2}(T)]\downarrow$$

where M_n describes the magnetic moment of Fe^{3+} ion in the nth sublattice. At 5 K, the values of saturation magnetization were observed to be quite high as compared to the values obtained at room temperature. Lu et al. [15] have discussed a model in which the dependence of magnetization on the particle size has been discussed with the equation as below:

$$\frac{M_s(D)}{M_{s0}} = 4\left\{1 - \frac{1}{2D/(Ch) - 1}\right\} \times \exp\left\{-\frac{2S_b}{3R}\frac{1}{2D/(Ch) - 1}\right\} - 3 \tag{4}$$

Therefore in accordance with Eq. (4) increase in particle size leads to the increase in $M_s(D)$. As in the present work particle size has been increasing with the substitution of La^{3+} ions thereby increase in magnetization has been justified.

Further, increase in M_s can be correlated to the anisotropy as rare-earth ions are known to have large magneto-crystalline anisotropy and large magnetostriction. Ounnunkad [16] has reported the decrease in magnetization after La=0.1, Sözeri et al. [11] and Cong-Ju Li et al. [9] reported the decrease in saturation magnetization with the increase in La^{3+} ions and the values obtained in the present work are quite high. Further, very high value of coercivity (5025.103 Oe) was observed for La=0.05. According to Cong-Ju Li et al. [9] for a material to be used in the longitudinal magnetic recording medium high coercivity (600 Oe) is required. If coercivity is too high, above 1200 Oe, the material can be used for the perpendicular recording media. So the present nanohexaferrites can be used in the perpendicular magnetic recording media. The magneto-crystalline anisotropy constant was calculated by using the following relation [17]:

$$K_1 = \mathrm{c}\, \mathrm{M}_s \times \mathrm{H}_a \tag{5}$$

where H_a is the anisotropy field and M_s is the saturation magnetization. Fig. 4 shows the variation of magneto-crystalline anisotropy as a function of La^{3+} substitution. K_1 was observed to increase, 1.45 x 10^6–1.54 x 10^6, with the increasing substitution of La^{3+} ions. The variations of K_1 can be qualitatively explained on the basis of single-ion anisotropy model [17], according to which Fe^{3+} ions present at A as well

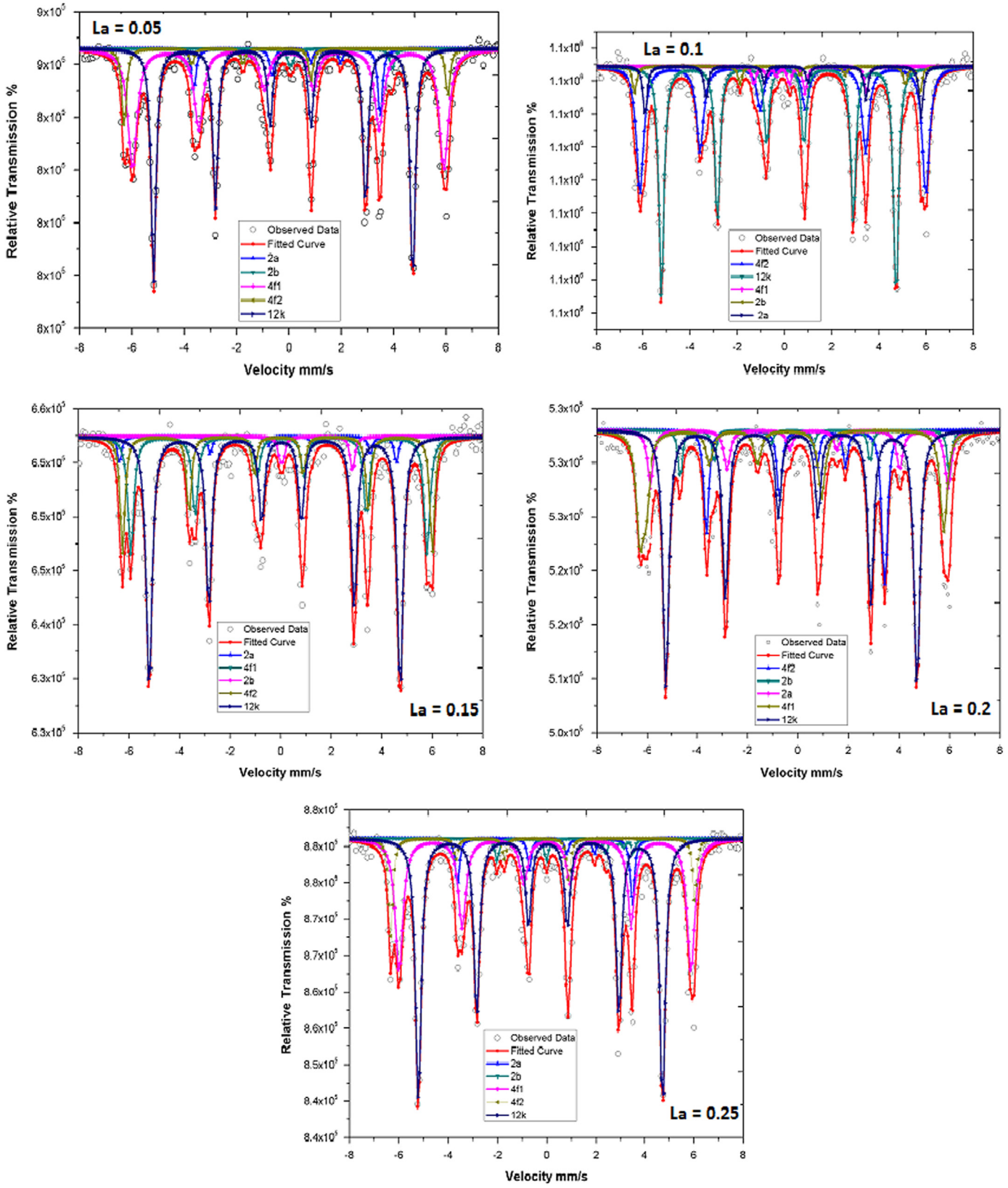

Fig. 5. Room temperature Mössbauer spectra for $BaLa_xFe_{12-x}O_{19}$ nanohexaferrites.

Table 3
Room temperature Mössbauer parameters for $BaLa_xFe_{12-x}O_{19}$ nanohexaferrites.

Site (sublattice)	x	WID (mm/s)	Isomer shift (mm/s)	Quadruple splitting	Hyperfine field	Total area (%)
12k (B-site)	0.05	0.24309	−0.10296	−0.27922	30.88233	46.22
	0.1	0.27553	−0.09895	−0.27026	30.87619	50.76
	0.15	0.28247	−0.09903	−0.27303	30.81329	49.08
	0.2	0.27799	−0.12141	−0.26303	30.87794	45.62
	0.25	0.27399	−0.09817	−0.27715	30.90077	48.81
4f1 (A-site)	0.05	0.35866	−0.06672	0.00471	37.62642	37.01
	0.1	0.27731	−0.03025	−0.0732	36.4218	23.67
	0.15	0.37493	−0.02886	−0.08036	36.66659	32.12
	0.2	0.33392	−1.40636	2.29237	37.52763	21.55
	0.25	0.38089	−0.02332	−0.05449	36.90526	33.79
4f2 (B-site)	0.05	0.194	0.00473	−0.12559	36.3298	8.08
	0.1	0.22598	−0.10084	−0.04993	38.08588	19.03
	0.15	0.194	−1.43041	2.60535	38.31441	8.33
	0.2	0.22289	0.62657	−1.39776	22.04857	15.37
	0.25	0.194	−1.4319	2.54739	38.49619	8.29
2a (B-site)	0.05	0.194	0.81507	2.7194	8.06233	4.36
	0.1	0.194	−0.2564	−1.28064	34.04297	3.87
	0.15	0.194	0.64117	−1.41251	22.03842	5.45
	0.2	0.30194	0.32859	−0.56707	36.69566	11.26
	0.25	0.194	0.65958	−1.41395	22.22102	6.15
2b (trigonal bipyramedal site)	0.05	0.194	0.65317	−1.91892	37.57601	4.33
	0.1	0.194	1.44211	−2.79938	0.42341	2.66
	0.15	0.194	0.97772	0.47272	29.84803	5.02
	0.2	0.194	0.22198	0.90383	33.11698	6.2
	0.25	0.194	0.97091	−3.97772	6.22551	2.97

as at B sites contribute to the anisotropy energy. Fe^{3+} ions present at tetrahedral sites ($4f_1$) and octahedral sites (2a, $4f_2$) give small positive contribution to the anisotropy. Fe^{3+} ions present on the octahedral site (12k) give very weak negative contribution and those present on the trigonal bipyramidal (2b) has largest positive contribution to the anisotropy [17]. As the concentration of La^{3+} ions is increased, the cation distribution of Fe^{3+} ions get modified which yields a different number of Fe^{3+} ions present at both the sites which in turn affect K_1. Increasing trend in K_1 with the increasing substitution of La^{3+} ions is justifying the observed behavior in saturation magnetization. The resonance of rotation magnetization, caused by the action of the anisotropic field (H_a), was calculated by using the following relation [17]:

$$f_r = \mathrm{H}_a\nu/2\pi \tag{6}$$

where ν is the gyromagnetic constant given by $\nu = 8.791 \times 10^6 g\ \mathrm{Oe}^{-1}\ \mathrm{s}^{-1}$, where g is the gyromagnetic ratio. Variation of f_r as a function of La^{3+} ions substitution is shown in Fig. 4. As the resonance is observed to occur at higher frequencies thus leads to the extended zone of utility for these nanohexaferrites.

3.3. Mössbauer study

Fig. 5 shows the room temperature Mössbauer spectra for $BaLa_xFe_{12-x}O_{19}$ (x=0.05, 0.1, 0.15, 0.2, 0.25) nanohexaferrites. The values of isomer shift, quadruple splitting and hyperfine field are listed in Table 3. As a result of the electrostatic interaction between the nucleus and electrons in a solid, the nuclear energy levels are shifted in both the source and the absorber. The shift is called isomer shift which can be represented as below:

$$\delta = \frac{2\pi}{5} Ze^2[|\varphi_a(0)|^2 - |\varphi_s(0)|^2]\left(R_{ex}^2 - R_{gd}^2\right) \tag{7}$$

where e is the electronic charge, Z is atomic number, R_{ex} is radius of the nucleus in the excited state, R_{gd} is radius of the nucleus in the ground state, $|\varphi_a(0)|^2$ is electron density evaluated at the nucleus for the absorber and $|\varphi_s(0)|^2$ is the electron density evaluated at the nucleus for the source. Since only s-electrons have a finite wave function at the nucleus and p and d electrons have vanishing wave functions at the nucleus, it is only the s-electrons which are responsible for the isomer shift. The isomer shift is a physical parameter for probing the valence state of a Mössbauer atom. It can be concluded from Table 3 that the observed value of average isomer shift is consistent with the presence of iron in 3^+ state. If the quadruple moment eQ of the ^{57}Fe nucleus in the absorber interacts with the electrical field gradient (EFG), the resulting interaction splits the excited state energy level into two lines, the splitting being called electric quadruple splitting (ΔE_Q). The quantity "e^2Qq" is called nuclear electric quadruple coupling constant. In the present work, quadruple splitting analysis indicates that there is non-uniform change in the values of quadruple splitting. The splitting in the Mössbauer spectrum which originates because of the coupling between the nuclear magnetic moment and the magnetic field at the nucleus is called hyperfine interaction or Zeeman splitting. The Hamiltonian for the hyperfine interaction can be expressed as

$$E_m = -g\mu_N M_\ell \tag{8}$$

where M_ℓ is the magnetic quantum number having $(2\ell+1)$ values, in accordance to this exchange interaction, the Mössbauer transition (six in number i.e. 4 sublevels for excited level l=3/2 and 2 sublevels for ground state l=1/2) takes place for various energy levels followed by selection rule $\Delta M_\ell = 0, \pm 1$. This hyperfine field interaction depends upon the particle size according to the following relation [18]:

$$H_{hf}(V,T) = H_{hf}(V=\infty,T)\left[1 - \frac{k_B T}{2KV}\right] \tag{9}$$

where k_B is the Boltzmann's constant, V is the particle volume and $V=\infty$, refers to a large crystals at temperature T in the absence of collective magnetic excitations. It is clear from Eq. (9) that hyperfine field increases with increase in particle size since particles with different volumes will show different hyperfine splitting. In M-type barium hexaferrites 12k sublattice has 6 Fe^{3+} ions [14]. Therefore due to larger number of Fe^{3+} ions the area of 12k sublattice is also large and is increasing the probability for La^{3+} ions to replace the Fe^{3+} ions at 12k sublattice. In fact the hyperfine field is small for 12k, therefore, the overall hyperfine field may be because of the difference between Fe^{3+} ions in spin up state and spin down state. The observed variations in the magnetic hyperfine field show that the increasing content of lanthanum ions is strengthening the super-exchange interactions.

4. Conclusion

Lanthanum substituted $BaFe_{12}O_{19}$ nanohexaferrites were successfully synthesized via sol–gel technique. The value of saturation magnetization and coercivity obtained in the present work were found to be high as compared to the values reported by other researchers. La^{3+} ions were observed to strengthen the super-exchange interactions of $BaFe_{12}O_{19}$ nanohexaferrite. It was observed that the synthesized nanoheferrites are very suitable for perpendicular magnetic recording media applications.

References

[1] S. Sharma, K.S. Daya, S. Sharma, M. Singh, Ultra low loss soft magnetic nanoparticles for applications up to S-band, Appl. Phys. Lett. 103 (2013) 112402.

[2] Gagan Kumar, S. Sharma, R.K. Kotnala, Jyoti Shah, Sagar E. Shirsath, Khalid M. Batoo, M. Singh, Electric, dielectric and ac electrical conductivity study of nanocrystalline cobalt substituted Mg–Mn ferrites synthesized via solution combustion technique, J. Mol. Struct. 1051 (2013) 336–344.

[3] Virender Pratap Singh, Gagan Kumar, R.K. Kotnala, Jyoti Shah, S. Sharma, K.S. Daya, Khalid M. Batoo, M. Singh, Remarkable magnetization with ultra-low loss $BaGd_xFe_{12-x}O_{19}$ nano-hexaferrites for applications upvto C-band, J. Magn. Magn. Mater. 378 (2015) 478–485.

[4] R.K. Kotnala, S. Ahmad, A.S. Ahmad, Jyoti Shah, A. Azam, Investigation of structural, dielectric, and magnetic properties of hard and soft mixed ferrite composites, J. Appl. Phys. 112 (2012) 054323–054330.

[5] J. Matutes-Aquino, S. Diaz-castanon, Synthesis by coprecipitation and study of barium hexaferrite powders, Scr. Mater. 42 (2000) 295.

[6] R.S. Alam, M. Moradi, M. Rostami, H. Nikmanesh, R. Moayedi, Y. Bai, Structural, magnetic and microwave absorption properties of doped Ba-hexaferrite nanoparticles synthesized by co-precipitation method, J. Magn. Magn. Mater. 381 (2015) 1–9.

[7] S.K. Chawla, R.K. Mudsainiyan, S.S. Meena, S.M. Yusuf, Sol–gel synthesis, structural and magnetic properties of nanoscale M-type barium hexaferrites $BaCo_xZr_xFe_{12-2x}O_{19}$, J. Magn. Magn. Mater. 350 (2014) 23–29.

[8] J. Lee, Yang-Ki Hong, W. Lee, G.S. Abo, J. Park, N. Neveu, Won-Mo Seong, Sang-Hoon Park, Won-Ki Ahn, Soft M-type hexaferrite for very high frequency miniature antenna applications, J. Appl. Phys. 111 (2012) 07A520.

[9] Cong-ju Li, Bin Wang, Jiao-Na Wang, Magnetic and microwave absorbing properties of electro spun $Ba_{(1-x)}La_xFe_{12}O_{19}$ nanofibers, J. Magn. Magn. Mater. 324 (2012) 1305–1311.

[10] V.N. Dhage, M.L. Mane, M.K. Babrekar, C.M. Kale, K.M. Jadhav, Influence of chromium substitution on structural and magnetic properties of $BaFe_{12}O_{19}$ powder prepared by sol–gel auto combustion method, J. Alloy. Compd. 509 (2011) 4394–4398.

[11] H. Sözeri, İ. KüÇük, H. Özkan, Improvement in magnetic properties of La substituted $BaFe_{12}O_{19}$ particles prepared with an unusually Fe/Ba molar ratio, J. Magn. Magn. Mater. 323 (2011) 1799–1804.

[12] G.M. Rai, M.A. Iqbal, K.T. Kubra, Effect of Ho^{3+} substitutions on the structural and magnetic properties of $BaFe_{12}O_{19}$ hexaferrites, J. Alloy. Compd. 495 (2010) 229.

[13] Gagan Kumar, Jyoti Shah, R.K. Kotnala, Virender Pratap Singh, Sarveena Godawari Garg, Sagar E. Shirsath, Khalid M. Batoo, M. Singh, Superparamagnetic behaviour and evidence of weakening in super-exchange interactions with the substitution of Gd^{3+} ions in the Mg–Mn nanoferrite matrix, Mater. Res. Bull. 63 (2015) 216–225.

[14] Virender Pratap Singh, Gagan Kumar, Jyoti Shah, Arun Kumar, M. Dhiman, R.K. Kotnala, M. Singh, Investigation of super-exchange interactions in $BaHo_xFe_{12-x}O_{19}$ $(0.1 \le x \le 0.4)$ nanohexaferrites and exploration at ultra high frequency region, Ceram. Int. 41 (2015) 11693–11701.

[15] H.M. Lu, W.T. Zheng, Q. Jiang, Saturation magnetization of ferromagnetic and ferromagnetic nanocrystals at room temperature, J. Phys. D.: Appl. Phys. 40 (2007) 320–325.

[16] S. Ounnunkad, Improving magnetic properties of barium hexaferrites by La or Pr substitution, Solid State Commun. 138 (2006) 472–475.

[17] Gagan Kumar, J. Chand, Anjana Dogra, R.K. Kotnala, M. Singh, Improvement in electrical and magnetic properties of mixed Mg–Al–Mn ferrite system synthesized by citrate precursor technique, J. Phys. Chem. Solids 71 (2010) 375–380.

[18] Gagan Kumar, Jyoti Shah, R.K. Kotnala, Virender Pratap Singh, M. Dhiman, Sagar E. Shirsath, M. Shahbuddin, Khalid M. Batoo, M. Singh, Mössbauer spectroscopic analysis and temperature dependent electrical study of $Mg_{0.9}Mn_{0.1}Gd_yFe_{2-y}O_4$ nanoferrites, J. Magn. Magn. Mater. 390 (2015) 50–55.